

The Arabidopsis PHOSPHATE 1 exporter undergoes constitutive internalization via clathrin-mediated endocytosis

Pallavi V. Vetal  and Yves Poirier* 

Department of Plant Molecular Biology, University of Lausanne, 1015 Lausanne, Switzerland

Received 4 June 2023; revised 11 August 2023; accepted 16 August 2023; published online 28 August 2023.

*For correspondence (e-mail yves.poirier@unil.ch).

SUMMARY

Inorganic phosphate (Pi) homeostasis is essential for plant growth and depends on the transport of Pi across cells. In *Arabidopsis thaliana*, PHOSPHATE 1 (PHO1) is present in the root pericycle and xylem parenchyma where it exports Pi into the xylem apoplast for its transfer to shoots. PHO1 consists of a cytosolic SPX domain followed by membrane-spanning α -helices and ends with the EXS domain, which participates in the steady-state localization of PHO1 to the Golgi and *trans*-Golgi network (TGN). However, PHO1 exports Pi across the plasma membrane (PM), making its localization difficult to reconcile with its function. To investigate whether PHO1 transiently associates with the PM, we inhibited clathrin-mediated endocytosis (CME) by overexpressing *AUXILIN-LIKE 2* or *HUB1*. Inhibiting CME resulted in PHO1 re-localization from the Golgi/TGN to the PM when PHO1 was expressed in Arabidopsis root pericycle or epidermis or *Nicotiana benthamiana* leaf epidermal cells. A fusion protein between the PHO1 EXS region and GFP was stabilized at the PM by CME inhibition, indicating that the EXS domain plays an important role in sorting PHO1 to/from the PM. PHO1 internalization from the PM occurred independently of AP2 and was not influenced by Pi deficiency, the ubiquitin-conjugating E2 PHO2, or the potential ubiquitination of cytosolic lysines in the EXS domain. PM-stabilized PHO1 showed reduced root-to-shoot Pi export activity, indicating that CME of PHO1 may be important for its optimal Pi export activity and plant Pi homeostasis.

Keywords: clathrin, endocytosis, Golgi, PHO1, phosphate, plasma membrane, transport.

INTRODUCTION

Plants import mineral nutrients from the soil that are crucial for their growth and development. The acquisition of different ions by roots and their translocation to aerial tissues is a critical aspect of plant ion homeostasis. Of the 13 mineral nutrients required by plants, phosphorus (P) is one of the main elements limiting growth and productivity (Poirier et al., 2022). Plants acquire P in the form of inorganic orthophosphate (Pi) and function as a structural element in nucleic acids and phospholipids, in energy metabolism as well as in the regulation of enzymes and signaling pathways. Pi limitation induces broad changes in gene expression and protein accumulation, leading to different developmental and metabolic acclimatory responses to improve Pi acquisition, storage, and remobilization (Dissanayaka et al., 2021; Gutiérrez-Alanís et al., 2018; Zhang et al., 2014).

The uptake of Pi into roots and its export to vascular tissues are essential for Pi homeostasis. Following its acquisition by the root system via PHOSPHATE TRANSPORTER 1 (PHT1) H⁺-Pi co-transporters (Nussaume et al., 2011), Pi is loaded into xylem vessels by PHOSPHATE 1

(PHO1) for its root-to-shoot transfer (Poirier et al., 1991; Hamburger et al., 2002). Arabidopsis (*Arabidopsis thaliana*) PHO1 is expressed in the root pericycle and xylem parenchyma cells (Arpat et al., 2012; Hamburger et al., 2002). PHO1 expression in ectopic plant tissues, such as leaf mesophyll cells, leads to the rapid and specific export of Pi to the apoplast (Arpat et al., 2012; Wege et al., 2016). Further support for the activity of PHO1 as a Pi exporter was obtained by the heterologous expression of rice (*Oryza sativa*) PHO1 orthologs in both mammalian cell cultures and *Xenopus laevis* oocytes (Ma et al., 2021). The Arabidopsis *pho1* mutant is defective in Pi translocation from roots to shoots and displays pleiotropic phenotypes expected for Pi deficiency, such as reduced shoot and root biomass and greater anthocyanin accumulation (Poirier et al., 1991). PHO1 has also been implicated in the transfer of Pi from maternal tissues to the embryo in both rice and Arabidopsis (Ma et al., 2021; Vogiatzaki et al., 2017). PHO1 orthologs in barrel clover (*Medicago truncatula*) mediate Pi transfer from infected nodule cells to nitrogen-fixing bacteria (Nguyen et al., 2020).

PHO1 is composed of an N-terminal hydrophilic tripartite SPX (SYG1/Pho81/XPR1) domain that binds inositol pyrophosphate, an important mediator of Pi sensing and signaling (Jung et al., 2018; Wild et al., 2016), followed by four transmembrane-spanning α -helices (4TM) and a hydrophobic C-terminal EXS (ERD1/XPR1/SYG1) domain (Wege et al., 2016). PHO1 is primarily localized to the Golgi and partially to the trans-Golgi network (TGN) at steady-state levels in root pericycle cells as shown by the expression of a complementing *PHO1-GFP* fusion construct in the *pho1* mutant (Arpat et al., 2012; Liu et al., 2012). The same Golgi and TGN localization of PHO1 is observed when *PHO1-GFP* is transiently expressed in *Nicotiana benthamiana* leaf epidermal cells and mediates specific Pi export (Arpat et al., 2012). These observations are in contrast to other transporters expressed in the root pericycle and involved in root-to-shoot ion transfer, such as REQUIRES HIGH BORON 1 (BOR1, for boron [B⁻]; Takano et al., 2002; Takano et al., 2005), NITRATE TRANSPORTER 1.5 (NRT1.5, for nitrate [NO₃⁻], Lin et al., 2008), NRT1/PTR FAMILY 2.4 (NPF2.4, for chloride ions [Cl⁻]; Li et al., 2016) and AMMONIUM TRANSPORTER 2;1 (AMT2;1, for ammonium ions [NH₄⁺]; Giehl et al., 2017), which localize to the plasma membrane (PM). The Golgi/TGN localization of PHO1 raises the question of how it mediates Pi export across the PM. As suggested by Arpat et al., 2012, one possibility is that only a minor fraction of PHO1 localizes to the PM to mediate Pi export. This situation would be analogous to that seen for the iron transporter IRON-REGULATED TRANSPORTER 1 (IRT1), which localizes to the TGN and early endosomes (EE) in root hair cells at steady-state levels and functions in the uptake of reduced (ferrous) iron from the extracellular space (Barberon et al., 2011). IRT1 was observed at the PM only when its recycling from the PM via endocytosis was inhibited by treatment with the drug tyrphostin A23 or by blocking monoubiquitination. However, such stabilization of IRT1 at the PM resulted in severe growth defects and oxidative stress due to metal toxicity (Barberon et al., 2011). An alternative hypothesis is that PHO1 mediates Pi export by loading Pi into Golgi-derived vesicles, followed by the release of Pi into the extracellular space through exocytosis (Arpat et al., 2012).

Among the endocytic pathways described to date, clathrin-mediated endocytosis (CME) is the most common pathway in plants (Dhonukshe et al., 2007). CME modulates the abundance of many transporters at the PM, such as IRT1, the NH₄⁺ transporter AMT1;3, the aquaporin PLASMA MEMBRANE INTRINSIC PROTEIN 2;1 (PIP2;1), the Pi transporter PHT1;1 and the manganese (Mn²⁺) transporter NATURAL RESISTANCE-ASSOCIATED MACROPHAGE PROTEIN 1 (NRAMP1), among others (Barberon et al., 2011, 2014; Castaigns et al., 2021; Li et al., 2011; Wang et al., 2013). CME requires an array of proteins, including heavy-chain and light-chain clathrins, together with adaptor and accessory

proteins (Aniento et al., 2022; McMahon & Boucrot, 2011; Paez Valencia et al., 2016; Rodriguez-Furlan et al., 2019). In plants, the classical hetero-tetrameric ADAPTOR PROTEIN 2 (AP2) complex functions as a clathrin adaptor for CME and is implicated in the recognition of select PM cargoes destined for CME via Tyr-based motifs (Bashline et al., 2013; Di Rubbo et al., 2013; Kim et al., 2013; Yamaoka et al., 2013; Yoshinari et al., 2019). The AP2 complex consists of two large subunits (α 2 and β 2 or AP2A and AP2B), one medium subunit (μ 2 or AP2M), and one small subunit (σ 2 or AP2S) (Collins et al., 2002).

In recent years, ubiquitination has emerged as a distinct signal recognized by the CME machinery to remove PM-localized plant proteins from the cell surface (Dubeaux & Vert, 2017; Ivanov & Vert, 2021). For instance, the ubiquitination of IRT1 and the Pi transporter PHT1;1 induces their internalization via CME (Barberon et al., 2011; Lin et al., 2013; Shin et al., 2013). Moreover, the TPLATE complex and TARGET OF MYB 1-LIKE (TOL) proteins have been shown to participate in the internalization of ubiquitinated plasma membrane cargos (Grones et al., 2022; Korbei et al., 2013; Moulinier-Anzola et al., 2020).

In this study, we addressed the role of CME in PHO1 localization using genetic strategies that block CME at the PM. We observed that PHO1 reaches the PM and undergoes constitutive cycling to internal vesicular compartments. We also show that the internalization of PHO1 by CME occurs independently of AP2. Stabilization of PHO1 at the PM in Arabidopsis was associated with reduced Pi export from the root to the shoot. Taken together, our findings provide evidence for the dynamic trafficking of PHO1 to and from the PM and suggest that this cycling is important for maintaining Pi homeostasis.

RESULTS

PHO1 is internalized from the PM via CME

To investigate whether PHO1 transits at the PM, we interfered with CME using a transient expression system in *N. benthamiana*. Overexpressing *AUXILIN-LIKE 2* inhibits CME by preventing the recruitment of clathrin to endocytic pits. This effect appears to be specific to the PM pool of clathrin without affecting the clathrin coating of other endosomal compartments (Adamowski et al., 2018). Accordingly, we co-expressed a *PHO1-GFP* (green fluorescent protein) construct along with a construct encoding either the Golgi marker MAN1 (α -1,2-MANNOSIDASE I)-mCherry, the TGN marker VT112 (VESICAL TRANSPORT V-SNARE 12)-mCherry or a PM-localized RFP (red fluorescent protein)-*AUXILIN-LIKE 2* in *N. benthamiana* leaf epidermal cells using separate binary vectors. As previously reported (Arpat et al., 2012), we observed a high level of co-localization for PHO1-GFP and the Golgi marker in larger fluorescent bodies and a lower level of co-localization between PHO1-GFP and

the TGN marker in the smaller and more mobile fluorescent bodies (Figure 1a,b). The transient expression of *AUXILIN-LIKE 2* led to the co-localization of PHO1-GFP with RFP-*AUXILIN-LIKE 2* at the PM (Figure 1c; Figure S1). To ensure that the observed effect of *AUXILIN-LIKE 2* expression on PHO1 re-localization to the PM was specific, we examined the effect of transient *AUXILIN-LIKE 2* expression on the localization of two other membrane-associated Golgi proteins, namely MAN1 (Nelson et al., 2007) and the phosphate transporter PHT4;6 (Cubero et al., 2009; Guo et al., 2008; Li et al., 2020). *AUXILIN-LIKE 2* expression did not shift the localization of these two Golgi membrane proteins towards the PM (Figure 1e,f; Figure S2).

Overexpressing a construct encoding the C-terminal part of CLATHRIN HEAVY CHAIN1 (called HUB1) has a dominant-negative effect on CME due to the binding of HUB1 to and out-titrating the clathrin light chains (CLCs) (Dhonukshe et al., 2007; Kitakura et al., 2011; Liu et al., 1995). To further assess the contribution of CME to PHO1 localization, we transiently co-expressed *PHO1-GFP* with *RFP-HUB1* in *N. benthamiana* leaves. As shown in Figure 1d, PHO1-GFP localized at the PM when its encoding construct was co-expressed with *RFP-HUB1*. Together, these results reveal that PHO1 localizes to the PM in *N. benthamiana* leaves when CME is inhibited.

Overexpressing *AUXILIN-LIKE 2* in Arabidopsis stabilizes PHO1 at the PM of root pericycle cells

To study the effect of inhibiting CME on the subcellular localization of Arabidopsis PHO1 in the root pericycle, we introduced the *XVE>>AUXILIN-LIKE 2* transgene from a previously characterized estradiol-inducible *XVE>>AUXILIN-LIKE 2* overexpressing line (Adamowski et al., 2018) into a *pho1-2* line complemented with a *pPHO1:PHO1-YFP* construct (hereafter referred to as line *pPHO1:PHO1-YFP_{compl.}*) to generate the *pPHO1:PHO1-YFP_{compl.} XVE>>AUXILIN-LIKE 2* line. In seedlings not expressing *AUXILIN-LIKE 2* (i.e., without estradiol treatment, DMSO mock control), PHO1-YFP showed a punctate pattern corresponding to the Golgi/TGN and some diffuse fluorescent signal likely representing protein degradation, with no signal visible at the PM (Figure 2a, upper panel). By contrast, upon estradiol induction, we observed a decrease in the PHO1-YFP punctate pattern and a significant increase in the PHO1-YFP signal at the PM that co-localized with the PM marker tdTomato-RCI2A (RARE-COLD-INDUCIBLE 2A) (Zhou et al., 2020; Figure 2a, lower panel). Confocal cross-section images along with intensity line plots (Figure 2b,c) showed a shift of PHO1-YFP from the endomembranes to co-localization with the PM marker tdTomato-RCI2A in root pericycle cells upon *AUXILIN-LIKE 2* induction. We confirmed the overexpression of *AUXILIN-LIKE 2* in these lines after estradiol induction by RT-qPCR analysis (Figure S3).

To evaluate if PHO1 could be stabilized at the PM when accumulating in a cell type other than root pericycle cells, we transformed Arabidopsis Col-0 and the *XVE>>AUXILIN-LIKE 2* overexpressing line with a construct encoding PHO1 fused to the fluorescent protein Dendra2 at its C-terminus under the control of an estradiol-inducible trichoblast-specific *WEREWOLF* promoter (*pWER>>XVE:PHO1-Dendra2*) (Lee & Schiefelbein, 1999; Siligato et al., 2016). In the presence of estradiol, we detected punctate-like structures in the epidermis of *pWER>>XVE:PHO1-Dendra2* cells that resembled native PHO1 localization in the root pericycle (Figure 2d, upper panel). The large PHO1-Dendra2 punctate structures co-localized well with the mCherry-GOT1 (GOLGI TRANSPORT 1) Golgi marker (Wave18R; Geldner et al., 2009), while smaller structures showed partial co-localization with the TGN marker mCherry-VTI12 (Wave13R; Geldner et al., 2009) (Figure S4a; Arpat et al., 2012). However, upon co-induction of *AUXILIN-LIKE 2* overexpression in the *AUXILIN-LIKE 2* dominant-negative line background, we observed accumulation of PHO1-Dendra2 at the PM (Figure 2d, lower panel). We did not observe any fluorescent signal in these lines after mock (DMSO) treatment (Figure S4b). These results suggest that PHO1 can cycle between the PM and Golgi/TGN in root cells other than the pericycle and that this dynamic localization is controlled by endocytosis via a CME pathway.

Stabilization of PHO1 at the PM leads to reduced ³³Pi translocation from root to shoot

We investigated the effects of PM stabilization of PHO1 on its root-to-shoot Pi transfer function by analyzing the translocation of radiolabeled ³³Pi in the shoots of *pPHO1:PHO1-YFP_{compl.} XVE>>AUXILIN-LIKE 2*. Since the repression of CME in this line is not limited to the root pericycle, we first examined the effects of *AUXILIN-LIKE 2* overexpression on the uptake of ³³Pi from the medium to examine its possible influence on root Pi import. To this end, we transferred *pPHO1:PHO1-YFP_{compl.} XVE>>AUXILIN-LIKE 2* and control (*pho1-2 XVE>>AUXILIN-LIKE 2*, Col-0 and *pho1-2*) plants grown for 6 days on medium containing 0.625 μM Pi to the same medium supplemented with estradiol for *AUXILIN-LIKE 2* induction or DMSO (mock control). Following 16 h of treatment, we exposed the roots to medium containing 10 μM Pi and 3 μCi ³³Pi with or without estradiol and calculated the total amount of ³³Pi acquired by the root by measuring the radioactivity present in the whole seedlings (shoot and root) per root mg fresh weight. Pi uptake by the root system decreased in response to the induction of *AUXILIN-LIKE 2* expression compared to the DMSO control (Figure 3a). To circumvent this situation, we increased the amounts of Pi and ³³Pi 10-fold only for estradiol-treated seedlings. Under these conditions, whereas both Col-0 and *pho1-2* seedlings showed increased ³³Pi uptake from

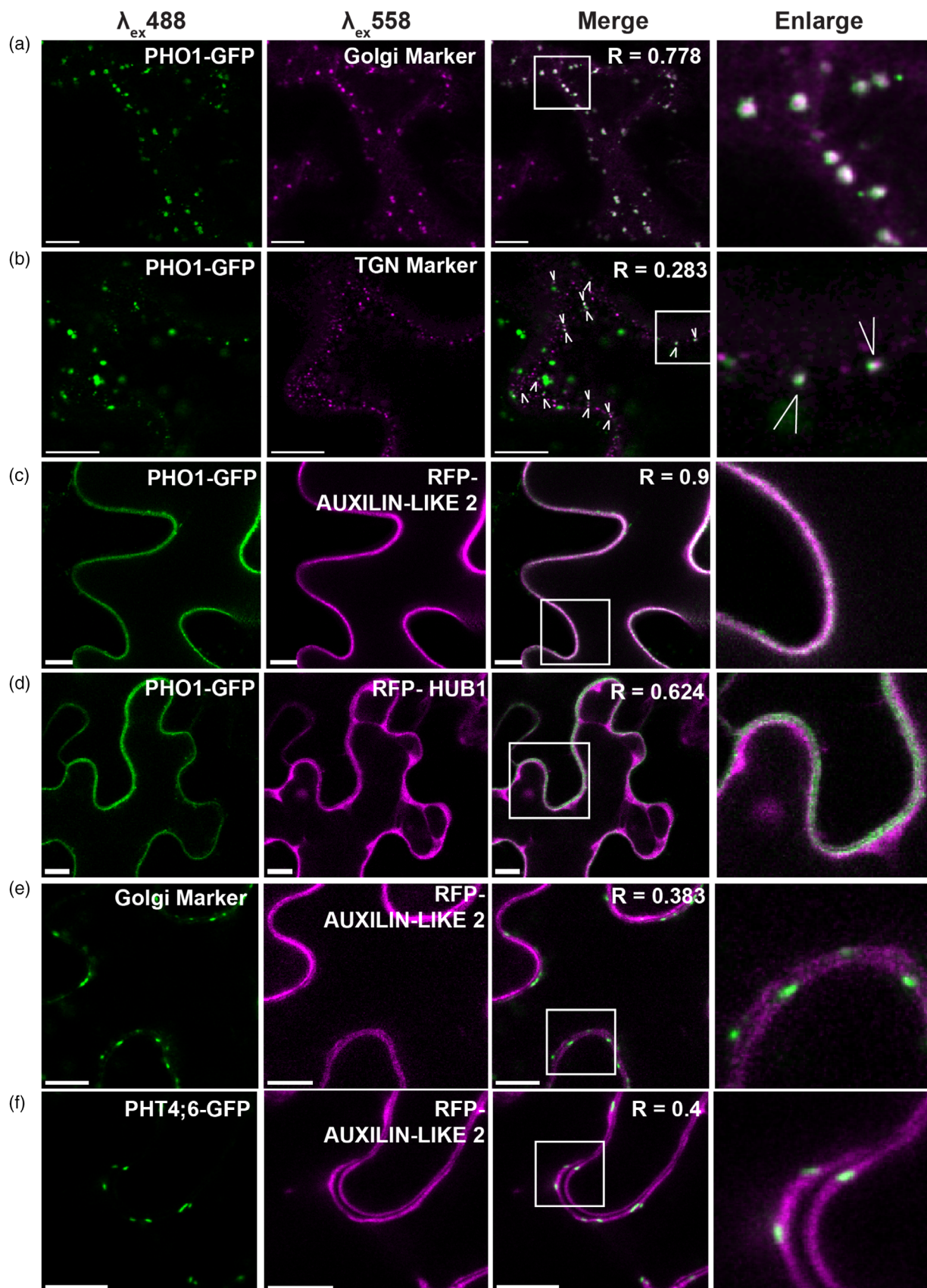


Figure 1. Overexpressing *AUXILIN-LIKE 2* or *HUB1* stabilizes PHO1-GFP at the plasma membrane in *N. benthamiana*. (a, b) Subcellular co-localization of full-length PHO1-GFP with markers for (a) the Golgi (MAN1-mCherry) or (b) TGN (VTI12-mCherry) in *N. benthamiana* epidermal cells. (c, d) Co-expression of PHO1-GFP with (c) RFP-*AUXILIN-LIKE 2* and (d) RFP-*HUB1*. (e, f) MAN1-GFP and PHT4;6-GFP (f) remain localized to the Golgi in cells co-expressing RFP-*AUXILIN-LIKE 2*. White arrowheads in b indicate partial co-localization of PHO1 with the TGN marker. R, Pearson's correlation coefficient of co-localization. Scale bars, 10 μm .

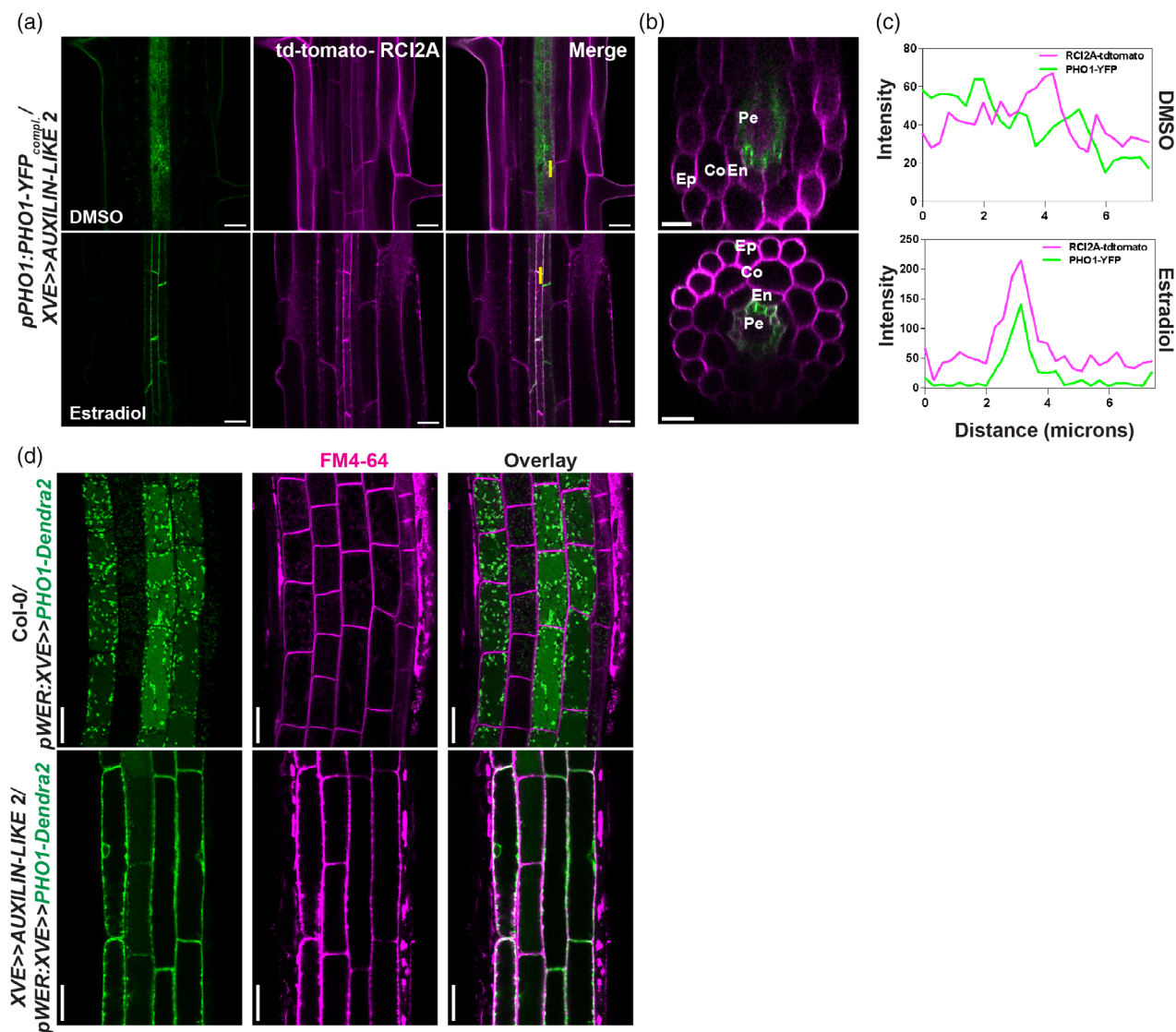


Figure 2. PHO1 internalization at the plasma membrane is regulated by CME. (a–c) A *pPHO1:PHO1-YFP_{compl}* line was crossed to an estradiol-inducible *XVE>>AUXILIN-LIKE 2* line. (a) Confocal image showing the stabilization of PHO1-YFP at the plasma membrane (PM) following *AUXILIN-LIKE2* overexpression in the root of a 6-day-old Arabidopsis seedling treated with estradiol (lower panels). Mock (DMSO) treatment had no effect on PHO1 localization (upper panels). (b) Cross-section of a DMSO-treated Arabidopsis root showing punctate-like structures of PHO1-YFP (upper panel) and PM localization at the pericycle in estradiol-treated roots (lower panels). Co, cortex; En, endodermis; Ep, epidermis; Pe, pericycle. (c) Line plot showing the corresponding fluorescence intensity of PHO1-YFP and RCI2A td-tomato (PM marker) in Arabidopsis roots. The signal intensity of DMSO-treated roots is shown in the upper panel and estradiol-treated roots in the lower panel. Fluorescence intensity is drawn from the vertical yellow lines shown in (a), right panels. (d) Subcellular localization of PHO1-Dendra2 encoded by a construct driving expression from an inducible epidermis-specific promoter (*pWER:XVE*) with (lower panels) or without (upper panels) *AUXILIN-LIKE 2* overexpression. In d, FM4-64 was used to define the PM of the epidermis. Scale bars, 20 μm .

medium containing estradiol, the amount of ^{33}P i acquired in the *XVE>>AUXILIN-LIKE 2* lines treated with estradiol matched that of the DMSO mock treatment (Figure 3b). We, therefore, used these conditions to evaluate the

long-distance root-to-shoot transfer of Pi. We calculated the root-to-shoot transfer capacity of seedlings as the ratio of ^{33}P i transferred to the shoot relative to the total amount of ^{33}P i acquired by the seedlings via their roots. We observed

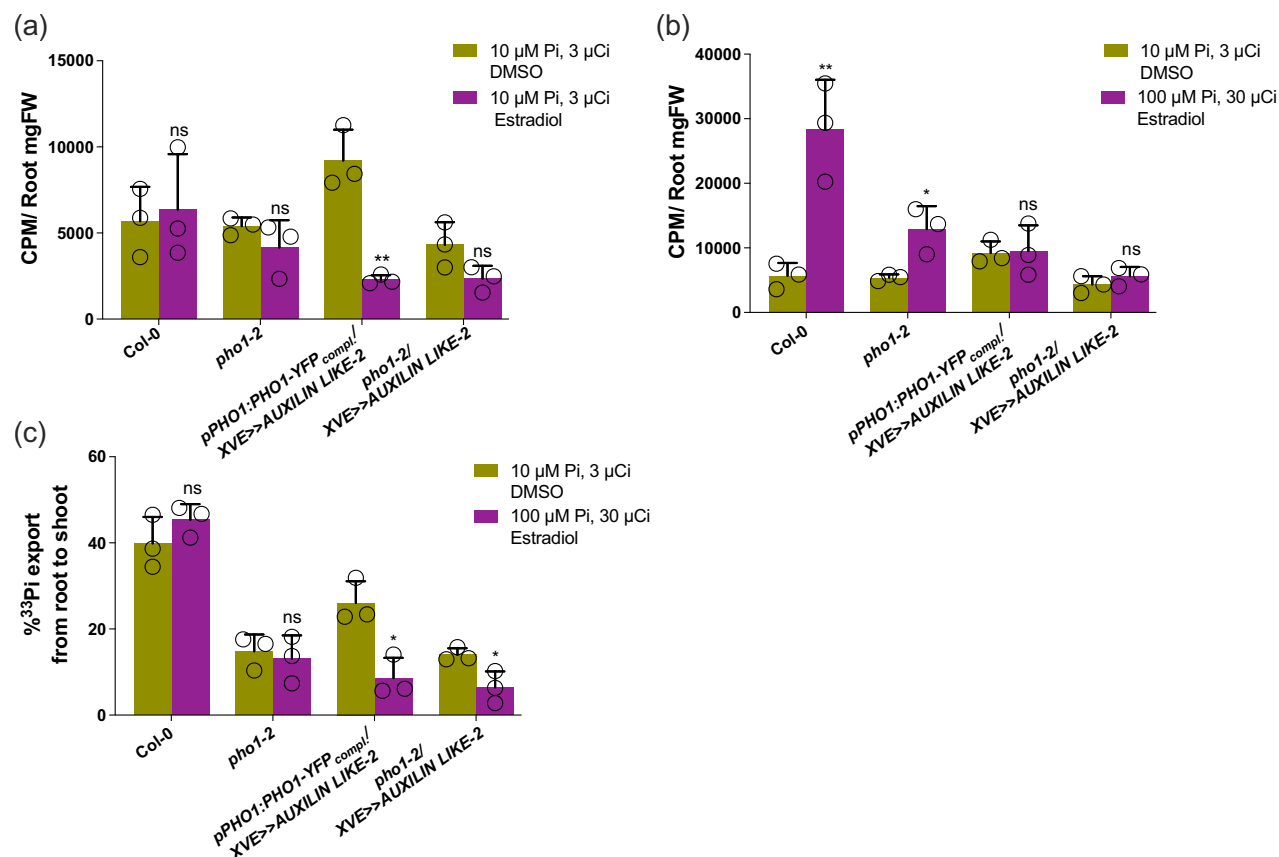


Figure 3. PHO1 stabilization at the PM affects Pi export from root to shoot. Col-0, *pho1-2*, *pho1-2 XVE>>AUXILIN-LIKE 2* and *pPHO1:PHO1-YFP_{compl}. XVE>>AUXILIN-LIKE 2* were grown on agar-solidified half-strength Murashige and Skoog medium (0.625 mM Pi) for 6 days before being transferred to plates containing the same medium supplemented with either 5 μM estradiol or 0.05% (v/v) DMSO (mock) for 16 h. The roots were subsequently immersed in liquid MS medium containing ^{33}P i and Pi for 1 h before quantification of ^{33}P i uptake and Pi transfer from roots to shoots. (a, b) Measurement of ^{33}P i import into the roots of seedlings on medium containing (a) 3 μCi ^{33}P i and 10 μM Pi with DMSO (black bars) or estradiol (gray bars) and (b) 30 μCi ^{33}P i and 100 μM Pi with DMSO (black bars) or 30 μCi ^{33}P i and 100 μM Pi with estradiol (gray bars). (c) Measurement of ^{33}P i export from root to shoot in seedlings treated with 3 μCi ^{33}P i and 10 μM Pi with DMSO (black bars) or 30 μCi ^{33}P i and 100 μM Pi with estradiol (gray bars). Data are means \pm standard deviation ($n = 3$, 10–12 plants were pooled for each biological replicate). Significant differences relative to the corresponding DMSO controls are indicated (** $P < 0.01$, * $P < 0.05$; Student's t -test).

a ~67% drop in the export of ^{33}P i from roots to shoots in estradiol-induced *pPHO1:PHO1-YFP_{compl}. XVE>>AUXILIN-LIKE 2* seedlings compared to the non-induced DMSO-treated controls (Figure 3c). The export of ^{33}P i from roots to shoots in seedlings where *AUXILIN-LIKE 2* was induced in the *pho1-2* mutant background also decreased to a similar extent (~54%). By contrast, we observed no reduction in root-to-shoot ^{33}P i transfer in estradiol-treated Col-0 or *pho1-2* seedlings compared to their respective mock controls (Figure 3c). These results indicate that induction of *AUXILIN-LIKE 2* negatively impacts root-to-shoot Pi transfer independently from its effect on root Pi uptake.

Although the export of Pi into the root xylem is primarily mediated by PHO1, its closest homolog PHO1;H1 also contributes to Pi loading to the xylem (Stefanovic et al., 2007). Hence, to determine whether the reduced Pi transfer from roots to shoots in *pho1-2* is potentially associated with the localization of PHO1;H1 at the PM due to *AUXILIN-LIKE 2*-mediated CME inhibition, we generated

lines expressing *PHO1;H1-GFP* under the control of the *PHO1* promoter in the *pho1-2 XVE>>AUXILIN-LIKE 2-mCherry* background. Confocal microscopy showed that under mock treatment, PHO1;H1-GFP localizes to punctate-like structures, with a diffuse fluorescent signal likely representing protein degradation, with no signal at the PM visible in the root vasculature, similar to PHO1-YFP (Figure S5, left panel). By contrast, we observed a change in the localization of PHO1;H1-GFP to the PM when we induced *AUXILIN-LIKE 2* overexpression by the addition of estradiol (Figure S5, right panel).

CME of PHO1 occurs independently of AP2

The clathrin-dependent internalization of PHO1 from the PM prompted us to study the role of the AP2 complex in PHO1 endocytosis. Since the Arabidopsis *ap2m-1* mutant lacking the μ subunit of AP2 shows defects in endocytosis (Bashline et al., 2013), we examined the subcellular localization of PHO1-GFP in the *ap2m-1* background harboring a

pPHO1:PHO1-GFP transgene. We did not observe any change in PHO1-GFP localization in the vasculature of *ap2m-1* (Figure 4a). The *ap2m-1* mutant has longer primary

roots and defects in internalization of the endocytic tracer dye FM4-64 compared to the wild type (Bashline et al., 2013, 2015); we observed the same features in *ap2m-*

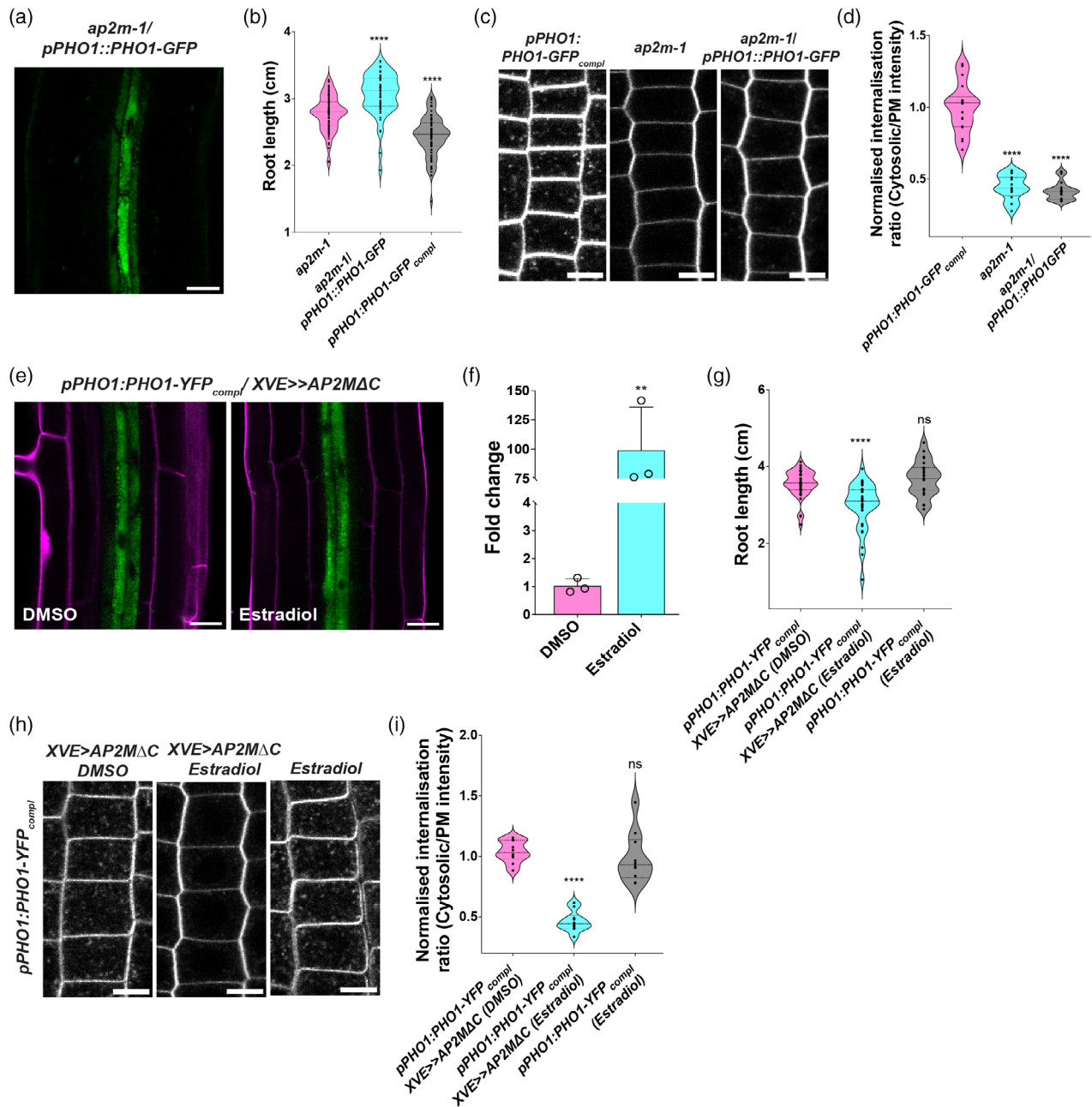


Figure 4. CME of PHO1 occurs independently of AP2. (a) Subcellular localization of PHO1-GFP in the roots of *ap2m-1*. (b) Measurement of root length in 7-day-old *pPHO1:PHO1-GFP_{compl.}*, *ap2m-1* and *ap2m-1 pPHO1:PHO1-GFP* seedlings. ANOVA **** $P < 0.0001$, $n = 50-70$ roots per genotype. (c) Imaging of FM4-64 puncta in the epidermal root cells of *pPHO1:PHO1-GFP_{compl.}*, *ap2m-1* and *ap2m-1 pPHO1:PHO1-GFP* seedlings. (d) Quantification of the ratio of intracellular-to-PM FM4-64 signal intensity normalized to that of the *pPHO1:PHO1-GFP_{compl.}* control. ANOVA **** $P < 0.0001$, $n = 10-15$ (~8 cells) roots per genotype. (e) Localization of PHO1-YFP after mock (DMSO) or estradiol induction of *AP2MΔC* expression (5 μ M estradiol for 2 days). Propidium iodide staining (magenta) was used to define cell boundaries. (f) RT-qPCR analysis of *AP2M* expression in *pPHO1:PHO1-YFP_{compl.} XVE>>AP2MΔC* seedlings following induction with 5 μ M estradiol for 2 days. Relative expression level after mock treatment (DMSO only) was set to 1. Student's *t*-test, ** $P < 0.01$, $n = 3$ biological replicates. (g) Root length of *pPHO1:PHO1-YFP_{compl.}* and *pPHO1:PHO1-YFP_{compl.} XVE>>AP2MΔC* seedlings treated with estradiol or with an equivalent volume of DMSO (mock). Arabidopsis seeds were incubated for 7 days on inductive medium (5 μ M estradiol). ANOVA **** $P < 0.0001$, $n = 30-40$ roots per genotype. Confocal images (h) and quantification (i) of cytosolic-to-PM ratios of FM4-64 internalization in the genotypes mentioned in (g). ANOVA **** $P < 0.0001$, $n = 10-13$ (~8 cells) roots per genotype. Data are means \pm SD. Scale bars, 20 μ m.

1 carrying *pPHO1:PHO1-GFP* compared to the *pPHO1:PHO1-GFP_{compl.}* control (*pho1-2* complemented with the same *pPHO1:PHO1-GFP* construct) (Figure 4b–d).

To independently examine the role of AP2 in PHO1 localization, we genetically interfered with AP2 function by overexpressing the dominant-negative *AP2MΔC* construct, where the AP2M C-terminal end responsible for cargo binding is deleted, in the *pPHO1:PHO1-YFP_{compl.}* genetic background (Bashline et al., 2013; Di Rubbo et al., 2013; Kim et al., 2013; Yamaoka et al., 2013). Upon induction of *AP2MΔC* expression, we did not detect any change in PHO1-YFP localization compared to the noninduced DMSO control (Figure 4e). RT-qPCR analysis showed that *AP2MΔC* is overexpressed 100-fold in seedlings treated with estradiol compared to mock treatment (Figure 4f). We also observed the decrease in root length and internalization of FM4-64 fluorescent puncta previously associated with the expression of *AP2MΔC* (Di Rubbo et al., 2013) in the *pPHO1:PHO1-YFP_{compl.} XVE>>AP2MΔC* line upon induction with estradiol relative to the DMSO control (Figure 4g–i). Altogether, these results indicate that the internalization of PHO1 via CME occurs independently of AP2.

PHO2 and the plant Pi status do not influence PHO1 localization

Pi availability affects PHO1 expression at both the transcriptional level and via ubiquitin-mediated degradation (Hamburger et al., 2002; Liu et al., 2012). We thus investigated if PHO1 localization is modulated by the plant Pi status by examining the localization of PHO1-YFP in the roots of seedlings grown for 6 days on Pi-sufficient or Pi-deficient medium. Confocal microscopy did not reveal a change in the localization of PHO1-YFP in roots under Pi-deficient conditions relative to Pi-sufficient conditions (Figure S6), suggesting that the dynamic cycling of PHO1 between the Golgi/TGN and PM does not depend on the availability of Pi in the medium.

PHO2 encodes a ubiquitin-conjugating E2 enzyme that ubiquitinates PHO1, leading to its degradation (Liu et al., 2012). To determine if *PHO2* influences the localization of PHO1, we transformed the *pho2* mutant with the *proPHO1:PHO1-YFP* construct and examined the localization of the encoded fusion protein by confocal microscopy. The punctate pattern associated with the Golgi/TGN localization of PHO1 in the *pho2* mutant background was similar to that seen in the *pho1-2* mutant, with no fluorescent signal associated with the PM (Figure 5a).

The effect of the EXS domain of PHO1 on PM localization is not dependent on ubiquitination

Previous studies on the structure of PHO1 showed that removing its C-terminal EXS domain resulted in the localization of the PHO1 truncated protein to the ER, while a fusion protein consisting of only the EXS domain of PHO1

fused to RFP resulted in co-localization with full-length PHO1-GFP to the Golgi/TGN (Wege et al., 2016). These findings highlight the important role of the EXS domain in the Golgi/TGN localization of PHO1. To investigate if the C-terminal EXS domain of PHO1 functions in its PM localization, we crossed the *pPHO1:EXS-GFP* line (producing only the EXS domain of PHO1 fused to GFP) with the *XVE>>AUXILIN-LIKE 2* line. Upon *AUXILIN-LIKE 2* overexpression by estradiol treatment, we observed stabilization of EXS-GFP at the PM in the pericycle compared to the DMSO control (Figure 5b). These results suggest that the C-terminal EXS domain of PHO1 functions in PHO1 trafficking to the PM.

The PHO2-mediated degradation of PHO1 implicates the ubiquitination of the N-terminal half of PHO1 harboring the SPX domain (Liu et al., 2012). Considering that PHO1 localization is not affected in the *pho2* mutant, in addition to our observation that the EXS domain of PHO1 was stabilized to the PM in response to *AUXILIN-LIKE 2* overexpression, we examined whether lysine residues in the EXS domain and the preceding four transmembrane regions (4TM domain) could be ubiquitination sites involved in the localization of PHO1 to the PM. Based on the previously described topology of PHO1 (Wege et al., 2016), we generated two PHO1 variants whose lysine residues facing the cytosol in the 4TM domain or EXS domain were changed to arginine residues. These variants contained mutations in three lysine residues in the 4TM region (K450R, K540R, and K548R) designated as TM K → R, and seven lysine residues (K583R, K591R, K677R, K685R, K687R, K700R, and K769R) in the EXS denoted as EXS K → R (Figure 6a; Figure S7). The K → R mutations in either the 4TM or EXS domain did not change the localization or function of PHO1 when we transiently expressed the encoding constructs in *N. benthamiana* leaves, as the variant proteins co-localized with Golgi and TGN markers (Figure 6b), and these lines showed greater Pi export to the apoplast compared to the empty vector control (Figure 6c). None of the PHO1 variants or controls showed any change in the level of nitrate exported to the medium, indicating that PHO1 specifically exports Pi.

Finally, we introduced GFP fusion constructs of these two TM K → R and EXS K → R PHO1 variants under the control of the *PHO1* promoter in the *pho1-2* mutant background to evaluate the effects of potential ubiquitination on the localization and Pi root-to-shoot transport activity of PHO1. Expressing the constructs encoding GFP fusions of both variants in the *pho1-2* background complemented the reduced shoot growth and low shoot Pi phenotypes of the *pho1-2* mutant to levels comparable to Col-0 and *pPHO1:PHO1-GFP_{compl.}* (Figure 7a,b). Both TM K → R and EXS K → R PHO1-GFP variants localized to punctate-like structures in the pericycle, similar to wild-type PHO1-GFP, which is indicative of Golgi/TGN localization (Figure 7c).

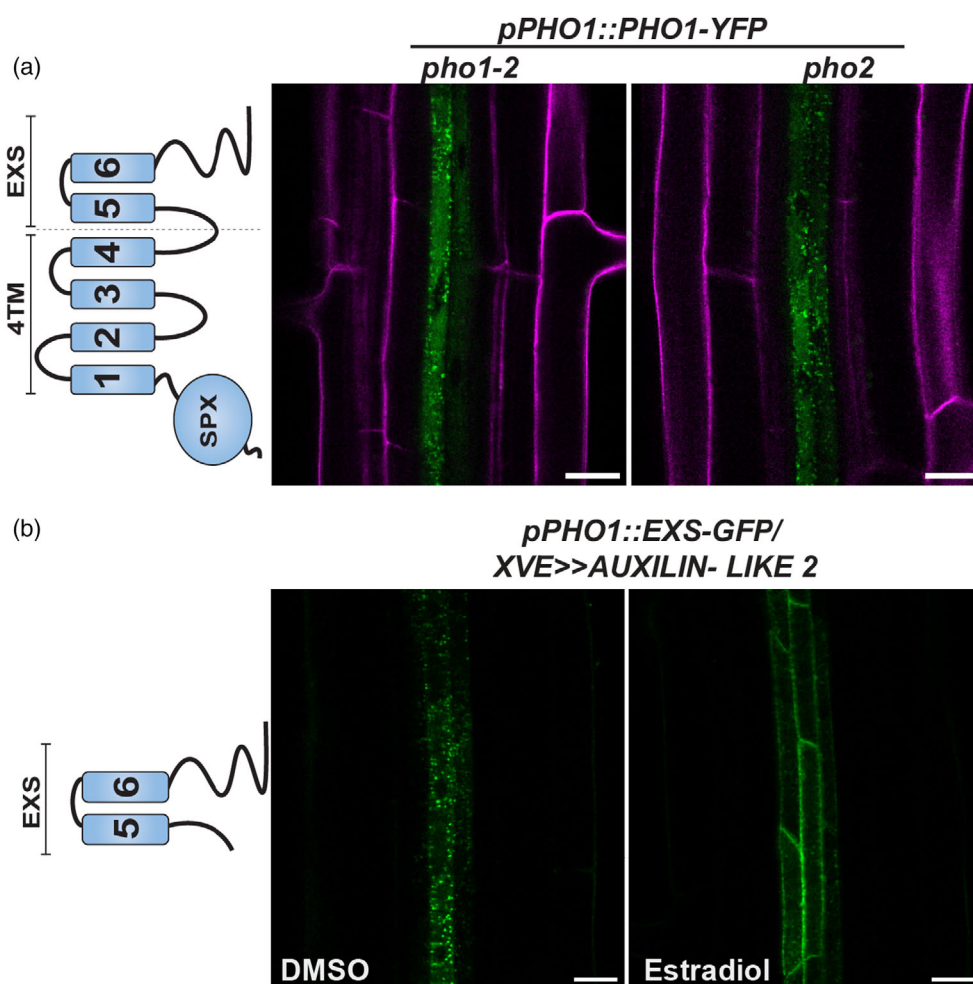


Figure 5. The EXS domain of PHO1 is involved in its trafficking from the Golgi/TGN to the plasma membrane. (a) Confocal microscopy of the localization of full-length PHO1-YFP in the *pho1-2* and *pho2* mutant backgrounds. A schematic diagram of PHO1-YFP (N-terminal SPX followed by four transmembrane α -helices [4TM] and ending with the EXS domain which includes the last two transmembrane α -helices) is shown on the left. Images show the overlay of GFP (green) and propidium iodide (magenta) fluorescence defining the cell wall boundaries. (b) Imaging of EXS-GFP in the roots of 6-day-old seedlings of the estradiol-inducible *AUXILIN-LIKE 2* overexpressor line treated with DMSO or estradiol for 16 h. All plants were grown in medium containing 0.625 μ M Pi. Scale bars, 20 μ m.

These results indicate that the ubiquitination of these lysine residues is not likely to be involved in regulating the localization of PHO1 to the PM.

DISCUSSION

Active internalization of PM-localized transporters via endocytosis has emerged as a powerful strategy to regulate ion homeostasis (Fuji et al., 2009; Ivanov & Vert, 2021; Zelazny & Vert, 2014). Here we demonstrated that endocytosis regulates the localization of the Pi exporter PHO1, since its PM localization only became apparent when we genetically impaired CME by overexpressing either *AUXILIN-LIKE 2* or *HUB1*. Importantly, localization of two other membrane-associated Golgi proteins, namely MAN1 and PHT4;6, was not modified by the overexpression of *AUXILIN-LIKE 2*. CME thus plays an important and specific

role in the trafficking of PHO1 between the Golgi/TGN and the PM. This mechanism was not cell-type specific, as we not only observed the shift in the subcellular localization of Arabidopsis PHO1 mediated by CME impairment in root pericycle cells (the endogenous expression domain of PHO1 in roots) but also when we ectopically expressed PHO1 in root epidermal cells and in *N. benthamiana* leaf epidermal cells. CME-mediated transporter internalization can be triggered by the abundance of the transporter substrate in the surrounding medium, representing a mechanism to regulate ion flux. Such CME-mediated internalization has been demonstrated for the plant transporters BOR1 by boron, NRAMP1 by manganese, and AMT1;3 by ammonium (Castaigns et al., 2021; Takano et al., 2002; Wang et al., 2013). Internalization of the PM-localized H^+ -Pi co-transporter PHT1;1 into endosomes for

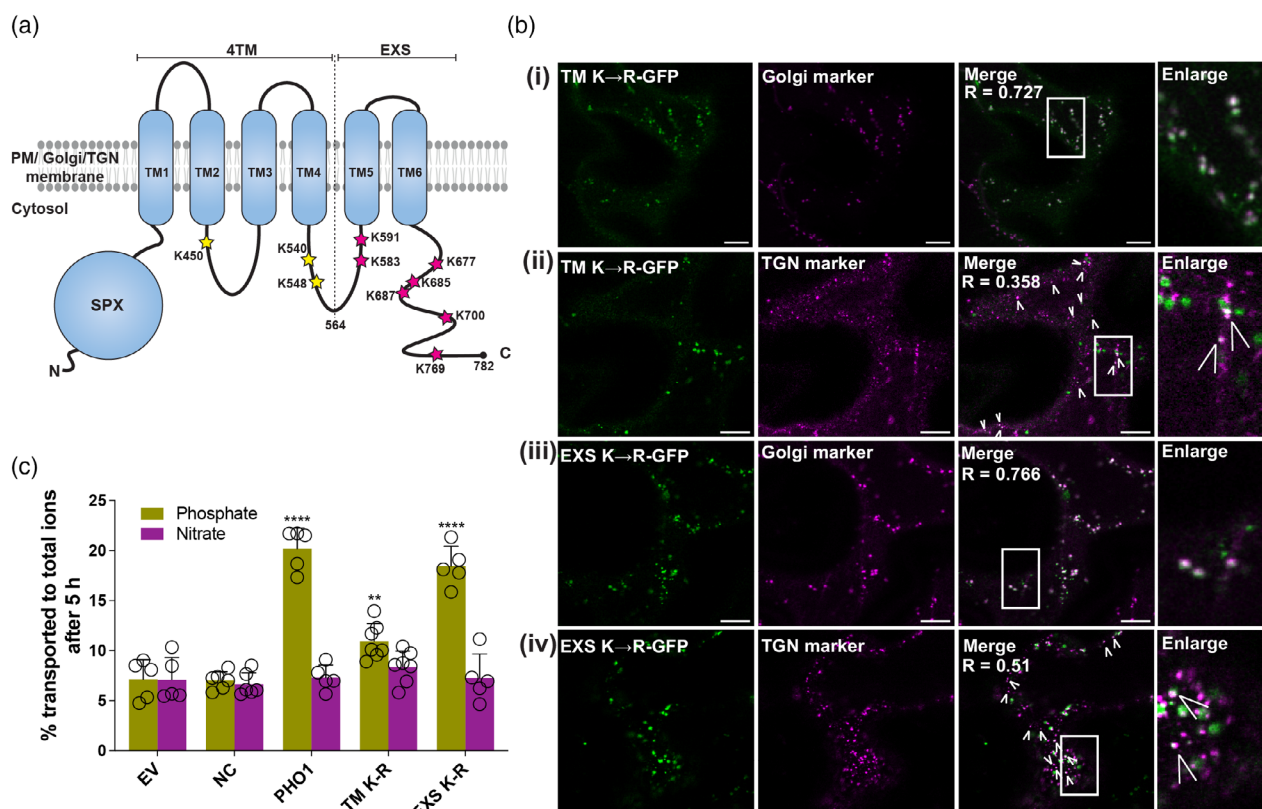


Figure 6. PHO1 TM K → R and EXS K → R mutants localize to the Golgi/TGN and export Pi into the extracellular space in *N. benthamiana* epidermal cells. (a) Topological model of Arabidopsis PHO1 showing the lysine residues (★) selected for mutagenesis. Two constructs encoding mutated PHO1-GFP were generated, one with three lysine-to-arginine mutations in the TM domain (TM K → R, ★ in yellow) and one with seven lysine-to-arginine mutations in the EXS domain (EXS K → R, ★ in magenta). (b) Subcellular localization of PHO1 mutants transiently expressed in *N. benthamiana*. Co-localization of TM K → R PHO1-GFP (i and ii) and EXS K → R PHO1-GFP (iii and iv) to the Golgi/TGN with Golgi (MAN1-mCherry, i and iii) or TGN (VTI12-mCherry, ii and iv) markers. White arrowheads point to partial co-localization of PHO1 mutants with the TGN marker. R (Pearson's correlation coefficient) values for co-localization are reported in each merged image. (c) Measurement of Pi and NO₃⁻ exported by PHO1 TM and EXS mutants transiently expressed in *N. benthamiana* leaf discs. The amounts of Pi and NO₃⁻ exported to the apoplast were measured after 5 h of incubation. Pi and NO₃⁻ export was measured in leaf discs expressing GFP or non-infiltrated (NC) leaf discs as a control. Data are means ± SD, *n* = 5, 4–5 discs were pooled for each biological replicate. Asterisks represent statistically significant differences compared to the empty vector control, ANOVA; *****P* < 0.0001; ***P* < 0.01. Scale bars, 10 μm.

subsequent degradation to the lytic vacuole occurs at high Pi in a process implicating the participation of ALIX, a cytosolic protein interacting with multivesicular bodies (MVBs) (Bayle et al., 2011; Cardona-López et al., 2015). By contrast, we did not detect a shift in PHO1 localization to the PM in pericycle cells of roots grown in either low- or high-Pi medium. CME-mediated internalization of PHO1 from the PM thus appears to be constitutive, at least under the conditions tested here.

Most key components of the CME machinery are conserved among plants, fungi, and animals (Baisa et al., 2013; Chen et al., 2011; Paez Valencia et al., 2016). The AP2M subunit of the AP2 complex has been implicated in the recognition of PM-localized protein cargoes destined for internalization (Bashline et al., 2013; Di Rubbo et al., 2013; Fan et al., 2013; Kim et al., 2013). The absence of PM localization for PHO1 in the dominant negative *AP2M1C* overexpressing line and the *ap2m-1* mutant suggests the existence

of an AP2-independent CME pathway for PHO1 internalization. AP2 is dispensable for plant endocytosis, as Arabidopsis mutants defective in single AP2 subunits remain viable (Bashline et al., 2013; Fan et al., 2013; Kim et al., 2013; Yamaoka et al., 2013). Mutations in the TPLATE complex (TPC) subunits are lethal, suggesting that this complex is an adaptor essential for CME (Gadeyne et al., 2014; Van Damme et al., 2007). Furthermore, one of the large subunits of the TPLATE complex has recently been shown to participate in the internalization of ubiquitinated plasma membrane cargo (Grones et al., 2022). Since the internalization of PHO1 appears to occur independently of the AP2 complex, it would be interesting to assess whether the TPC contributes to its internalization.

The C-terminal transmembrane region of PHO1, comprising the 4TM and EXS domains, was shown to be necessary and sufficient to mediate Pi export when transiently expressed in *N. benthamiana* (Wege et al., 2016).

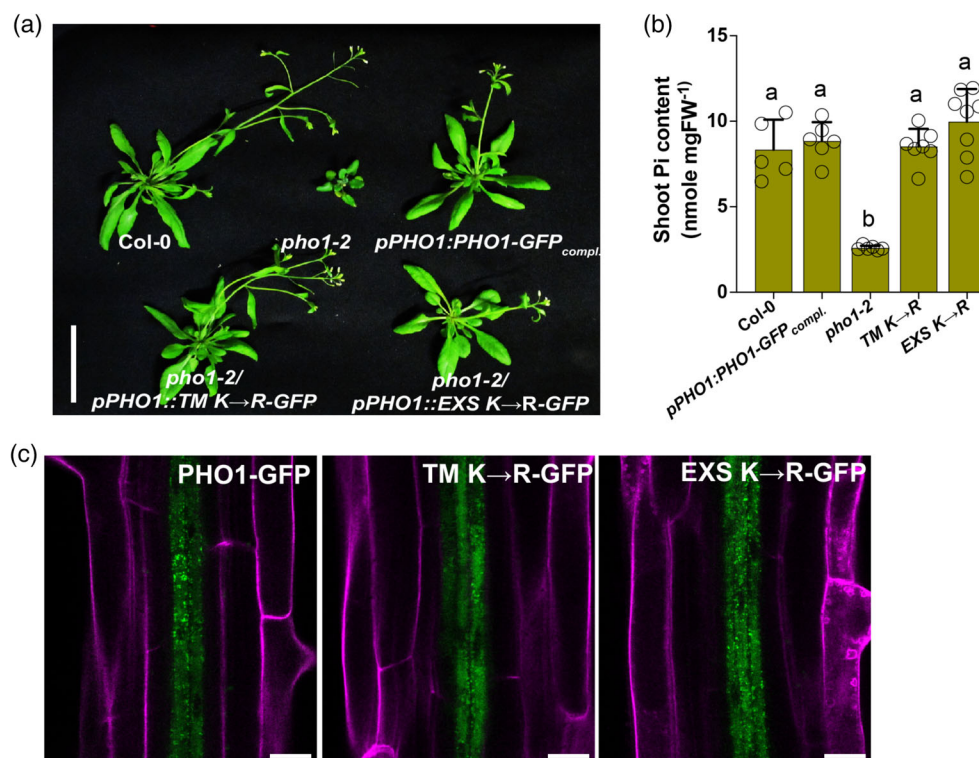


Figure 7. The potential ubiquitination sites in the cytosolic regions of PHO1 4TM and EXS do not control its internalization from the plasma membrane. (a) Phenotypes of plants transformed with constructs encoding each PHO1 K → R mutant in *pho1-2* compared to wild type (Col-0), *pho1-2*, and *pPHO1:PHO1-GFP_{compl}*. Plants were grown in pots for 32 days. Scale bar, 5 cm. (b) Pi contents of shoots from the lines mentioned in (a). Data are means ± SD, $n = 5-7$. For all histograms, different lowercase letters indicate significant differences, as determined by ANOVA with a Tukey Kramer test, $P < 0.05$. (c) GFP fluorescence in the root pericycles of *pho1-2* seedlings expressing full-length *PHO1-GFP*, TM K → R or EXS K → R mutant-GFP constructs. Images show the overlay of GFP (green) and propidium iodide (magenta) fluorescence defining the cell wall boundaries. Scale bars, 20 μm.

Furthermore, the EXS region was shown to be essential for the proper localization of PHO1 at the Golgi/TGN, and an EXS-RFP fusion protein co-localized with PHO1 (Wege et al., 2016). In the present study, we showed that inhibiting CME in seedling expressing an *EXS-GFP* fusion construct in the root pericycle also led to a shift of the fusion protein from the Golgi/TGN to the PM. Together, these results highlight the key role of the EXS domain of PHO1 in its localization and retrieval from the PM by CME.

Ubiquitination can trigger the internalization of transporters from the PM via CME. This observation was demonstrated by the ubiquitination of two lysine residues of IRT1 facing the cytosol (K154 and K179) by the E3 ubiquitin ligase IRT1 DEGRADATION FACTOR 1 (IDF1) (Barberon et al., 2011; Shin et al., 2013) and the action of the E3 ubiquitin ligase NITROGEN LIMITATION ADAPTATION (NLA) on PHT1 Pi importers (Lin et al., 2013). However, in the present study, mutating all the cytosol-facing lysine residues present in the 4TM or EXS region of PHO1 to arginine resulted in PHO1 variants still capable of complementing the *pho1* mutant. Moreover, these variant PHO1 proteins showed no shift in localization from the Golgi/TGN to the

PM in transient expression assays in *N. benthamiana* leaves or in root pericycle cells.

Beyond endocytosis, ubiquitination is also involved in controlling the levels of transporters via sorting to MVBs and lytic vacuoles. Ubiquitination of the N-terminal half of PHO1 (containing the SPX domain) by the ubiquitin-conjugating E2 enzyme PHO2 led to increased degradation of PHO1 via its targeting to MVBs (Liu et al., 2012). As a result, the *pho2* mutant shows high PHO1 abundance and exhibits constitutively active Pi starvation phenotypes, leading to excessive shoot Pi content and reduced growth (Aung et al., 2006; Bari et al., 2006). The identities of the lysine residues ubiquitinated in the SPX domain of PHO1 by PHO2 are unknown. However, our results indicate that the localization of PHO1 between the PM and Golgi/TGN is not affected in the *pho2* mutant, indicating that PHO2-mediated ubiquitination does not contribute to the CME of PHO1.

Stabilizing IRT1 at the PM by blocking ubiquitination resulted in an enhanced metal-importing activity of IRT1, leading to oxidative damage and strongly limited plant growth associated with the excessive accumulation of Fe and Mn⁺² (Barberon et al., 2011, 2014). These results

highlight the important role of IRT1 endocytosis in metal-importing activity, which is required for optimal metal homeostasis and plant survival. In an analogous manner, constitutive endocytosis can be seen as a way to prevent uncontrolled Pi export activity by PHO1. Overexpression of *PHO1* in leaves was previously shown to lead to the accumulation of very high levels of Pi in leaf xylem exudates, uncontrolled export of Pi into the leaf apoplastic space, and very poor growth, likely resulting from the metabolic costs of maintaining a futile cycle of Pi import and export (Stefanovic et al., 2011). In this context, it is surprising that the transient stabilization of PHO1 at the PM of the root pericycle via *AUXILIN-LIKE 2* induction led to a decrease in PHO1-mediated Pi export activity instead of an increase, which would be expected if the Pi export activity of PHO1 was mediated by a PM-localized protein. This impaired export activity might be associated with the lack of a partner protein or a posttranslational modification that would be required for PHO1 to be functionally active. Alternatively, this lower Pi export activity may be due to the absence of lateral polarity of the PM-stabilized PHO1. Several ion transporters have been shown to exhibit lateral polarity in root cells, which may be associated with more efficient radial transfer of ions across the root for vascular ion loading (Barberon & Geldner, 2014). Although the reason behind the lower Pi export activity of PM-stabilized PHO1 is currently unclear, these findings support a role for PHO1 internalization from the PM for its optimal activity in Pi transfer from root to shoot.

An attractive hypothesis for PHO1 Pi export activity is that this protein loads cytosolic Pi into Golgi-derived vesicles using both a differential Pi gradient and a charge gradient (generated by the vacuolar ATPase) as driving forces. Pi unloading to the apoplastic space would then occur through exocytosis to be followed by the rapid recycling of PHO1 from the PM by endocytosis and endosomal trafficking (Arpat et al., 2012). The spatial orientation of PHO1 (SPX and C-terminal end facing the cytosol; Wege et al., 2016) and driving forces mediating Pi export out of the cytosol would be similar whether PHO1 was localized at the PM, Golgi, or Golgi-derived vesicles. However, the vesicular hypothesis would explain the presence of a large fraction of PHO1 in the Golgi/TGN and its near absence at the PM, even under Pi-deficient conditions. The observed decrease in Pi export activity of PM-stabilized PHO1 may be explained by a reduction in the number of recycled endosomes available to participate in further rounds of vesicular Pi loading and export. Such a secretory pathway-mediated mechanism was previously proposed to explain how the trans-Golgi-localized Mn⁺² transporter METAL TOLERANCE PROTEIN 11 (MTP11) could be associated with elevated intracellular levels of Mn⁺² in the *mtp11* mutant and increased tolerance to excess Mn⁺² in plants overexpressing *MTP11* (Delhaize et al., 2007; Peiter et al., 2007). Support for such a synaptic-

like transport pathway in plants was recently described for the export of nicotianamine in vascular tissues via the NAET1/2 transporters (Chao et al., 2021). Whether PHO1 might export Pi via a similar synaptic-like pathway deserves further analysis.

MATERIALS AND METHODS

Plant materials and growth conditions

All *Arabidopsis thaliana* plants used in this study, including mutants and transgenic plants, were in the Columbia (Col-0) background. For the *in vitro* experiments, seeds were surface sterilized by chlorine gas and transferred to the square plates containing half-strength Murashige and Skoog (MS) salts (Duchefa M0255), 1% (w/v) sucrose, and 1% (w/v) agar in continuous light for 6 days. Seedlings were either used for confocal microscopy or transferred to soil and grown in long-day conditions (16 h of light and 8 h of dark at 20°C) for at least 25 days for phenotypic analysis and/or quantification of Pi content. For the Pi-deficient medium, MS salts without Pi (Caisson Labs, MSP11) were used. Pi buffer pH 5.7 (93.5% KH₂PO₄ and 6.5% K₂HPO₄) was added to obtain different Pi concentrations.

T-DNA insertion line *ap2m-1* (SALK_083693) (Fan et al., 2013; Kim et al., 2013; Yamaoka et al., 2013) was obtained from the Nottingham Arabidopsis Stock Centre. Previously published transgenic lines *Col-0 XVE>>AUXILIN-LIKE2* (Adamowski et al., 2018), *pho1-4 pPHO1::EXS-mGFP* (Wege et al., 2016), *pho1-2 pPHO1::PHO1-mGFP* (*pPHO1:PHO1-GFP_{compl.}*) (Wege et al., 2016), *pho1-2 pPHO1::PHO1-YFP* (*pPHO1:PHO1-YFP_{compl.}*) (Liu et al., 2012) and Wave marker line 13 and 18 (Geldner et al., 2009) were used for generating the crosses. Floral dip method was used for the generation of stable Arabidopsis transgenics (Clough & Bent, 1998). The constructs *XVE>>AP2M1C* (Di Rubbo et al., 2013), WT *pPHO1::PHO1-mGFP*, and mutated PHO1-GFP constructs were transformed into the line *pPHO1:PHO1-YFP_{compl.}*, *pho2* (Aung et al., 2006) and *pho1-2* (Hamburger et al., 2002) backgrounds, respectively.

Generation of constructs

PHO1 constructs with mutations at selected lysine residue in the 4TM and EXS domains were synthesized by GenScript ([genscript.com](https://www.genscript.com)). Genomic sequences of WT and mutated *PHO1* as well as the coding sequence of *C-HUB1* (Robert et al., 2010) were amplified and inserted into pENTR2B (Invitrogen) entry vector either by In-Fusion or Golden gateway strategy before being cloned into the binary plant expression vector pB7m34GW (Karimi et al., 2007) (modified with promoter *WEREWOLF* in the first and C-terminal Dendra2 fusion in the third position), pMDC32 (GFP C-fusion with the original 2X35S promoter or modified Arabidopsis *PHO1* native promoter) (Curtis & Grossniklaus, 2003) and pK7WGR2 (RFP N-fusion with the CaMV 35S promoter) respectively by LR reaction (Invitrogen). The Man1-RFP (Golgi) and VT112-mCherry (TGN) markers were previously described (Geldner et al., 2009; Nelson et al., 2007). The constructs were introduced into *Agrobacterium tumefaciens* pGV3101 and used for stable transformation in Arabidopsis by floral dipping (Clough & Bent, 1998) or transient expression in *Nicotiana benthamiana* (Arpat et al., 2012).

N. benthamiana infiltration and Pi export assay

Leaves of 4- to 5-week-old *N. benthamiana* plants were used for infiltration with *A. tumefaciens*. An overnight culture of

A. tumefaciens carrying constructs grown at 28°C was pelleted and resuspended in infiltration buffer containing 10 mM MgCl₂, 10 mM MES-KOH (pH 5.6), and 150 μM acetosyringone at a final OD₆₀₀ = 0.4 to 0.6. The cultures were incubated further for 1–2 h at 28°C on a shaker incubator. P19 expressed from a distinct binary vector was used to inhibit the silencing of the transgene. For coinfiltration, the *A. tumefaciens* strain carrying two constructs was mixed in an equal amount along with P19. Two days post-infiltration, leaves were cut randomly into 1-cm-diameter discs and taken either for confocal imaging or soaked in the buffer containing 5 mM glucose, 10 mM MES-KOH (pH 5.6), 1 mM KCl, 0.5 mM CaCl₂, 0.5 mM MgSO₄, and 0.01% Triton X-100 for Pi and NO₃⁻ export assay. Pi and NO₃⁻ released in the buffer were measured by the molybdate assay (Ames, 1966) and NO₃⁻ reductase assay (Barthes et al., 1995), respectively.

Pi content, ³³Pi import and ³³Pi root-to-shoot translocation assay in Arabidopsis

Pi levels in the shoot of soil-grown 4- to 5-week-old Arabidopsis were measured by releasing the cellular Pi content into the water by repeated freezing and thawing. Pi concentration was then quantified by molybdate assay using a standard curve.

To measure the uptake and transfer of ³³Pi from root to shoot, plants were first grown for 6 days on ½ MS medium containing 0.625 μM Pi. On day 7, plants were transferred to the same medium supplemented with 5 μM estradiol (dissolved in DMSO) or 0.05% (v/v) DMSO (mock control). Following 16 h of treatment, roots were incubated in liquid ½ MS with different concentrations of Pi and ³³Pi, ensuring that shoots do not touch the media. After 1 h, roots and shoots were separated, washed with ice-cold water and liquid ½ MS (1 mM Pi), blotted, and weighed before placing them in a scintillation vial with 10% SDS (w/v) for an hour at 55°C. Radioactivity in the tissue was measured using Ultima Gold scintillation liquid and the Perkin Elmer tri-carb 2800TF scintillation counter. Uptake rate was calculated as the total amount of radioactivity present in both roots and shoots divided by the weight of the roots. The percentage of transfer of Pi from roots to shoots was calculated as [shoot ³³Pi/(shoot ³³Pi + root ³³Pi)] × 100. No deleterious effects of estradiol treatment on root growth could be observed.

Chemical treatment

Five to six-day-old seedlings were transferred to ½ MS plates containing 5 μM estradiol or solvent (0.05% DMSO) for 16–20 h for transgene induction. For FM4-64 uptake experiments, seedlings were incubated in liquid ½ MS medium supplemented with 2 μM FM4-64 dye (Thermo Fisher) for 8 min in the dark and on ice. Excess dye was washed off and the seedlings were mounted in ½ MS medium on microscopy slides at room temperature for imaging and internalization measurement. Propidium iodide (Sigma-Aldrich) was diluted 100 times in ½ MS medium with 1% (w/v) sucrose and roots were stained for 2 min before confocal laser scanning microscopy (CLSM) imaging.

Confocal microscopy and quantification

CLSM images of Arabidopsis roots and *N. benthamiana* leaves for subcellular localization were taken with a Leica Stellaris, a Zeiss LSM700, or a Zeiss LSM880 confocal microscope. FM4-64 internalization was quantified using the ImageJ software. The ratio between the difference of the average cytosolic fluorescence intensity and the mean cytosolic background intensity (background subtracted cytosolic) and the mean plasma membrane

intensity was calculated. The average internalization ratio of each line was then normalized against the average internalization ratio of respective controls. Quantification of colocalization was conducted using the Fiji plugin JACoP (Bolte & Cordelières, 2006), in which Mander's coefficient and Pearson correlation coefficient were analyzed. Pearson correlation coefficient was calculated from a single CLSM image in the figure unless stated otherwise. Images were adjusted for color and contrast using ImageJ/Fiji software. Statistical analysis was done in Prism 9 (GraphPad Software, San Diego, CA, USA).

Quantitative RT-PCR

Total RNA from 7-day-old seedlings induced with 5 μM estradiol or DMSO control for 20 h was extracted using ReliaPrep™ RNA Miniprep Systems (Promega) according to manufacturer's instructions. Two micrograms of RNA was reverse-transcribed using M-MLV Reverse Transcriptase (M3681, Promega) and oligo d(T)₁₅ according to the manufacturer's instructions. qRT-PCR was performed using SYBR Select Master Mix (4 472 908, Applied Biosystems) with primer pairs specific to genes of interest and *EF1A* (At1g07940) used for data normalization. Relative gene expression was calculated with the 2^{-ΔΔCT} method (Livak & Schmittgen, 2001). Primer sequences are listed in Table S1.

ACKNOWLEDGEMENTS

The authors are grateful to Dr. Jiri Friml (Institute of Science and Technology Austria) as well as Drs. Daniel van Damme and Eugenia Russinova (VIB Belgium) for sharing clones and materials involved in CME. We also thank the Geldner group (University of Lausanne) for providing clones and advice. This work was supported by a grant from the Swiss National Science Foundation (31003A-182462) to YP. Open access funding provided by Université de Lausanne.

AUTHOR CONTRIBUTIONS

PVV and YP conceived the project and wrote the manuscript, and PVV performed all experiments. YP agrees to serve as the author responsible for contact and ensures communications.

CONFLICT OF INTEREST

The authors declare no conflict of interest.

DATA AVAILABILITY STATEMENT

All relevant data can be found within the manuscript and its supporting materials.

SUPPORTING INFORMATION

Additional Supporting Information may be found in the online version of this article.

Figure S1. Correlation coefficients between PHO1-GFP and RFP-AUXILIN-LIKE 2 expressed in *N. benthamiana* epidermal cells.

Figure S2. Localization of the Golgi proteins MAN1 and PHT4;6 is not modified by *AUXILIN-LIKE 2* overexpression.

Figure S3. Quantitative RT-PCR of *AUXILIN-LIKE 2*.

Figure S4. PHO1 localizes to Golgi and TGN in the epidermal cells of Arabidopsis roots.

Figure S5. Over-expression of *AUXILIN-LIKE 2* stabilizes the PHO1 homolog PHO1;H1 at the PM.

Figure S6. Subcellular localization of PHO1-YFP in roots grown under Pi-sufficient and Pi-deficient conditions

Figure S7. Arabidopsis PHO1 protein sequence with localization of mutated lysines.

Table S1. List of primers used in this study.

REFERENCES

- Adamowski, M., Narasimhan, M., Kania, U., Glanc, M., De Jaeger, G. & Friml, J. (2018) A functional study of AUXILIN-LIKE1 and 2, two putative clathrin uncoating factors in *Arabidopsis*. *Plant Cell*, **30**, 700–716.
- Ames, B.N. (1966) Assay of inorganic phosphate, total phosphate and phosphatases. *Methods in Enzymology*, **8**, 115–118.
- Aniento, F., de Medina, S., Hernández, V., Dagdas, Y., Rojas-Pierce, M. & Russinova, E. (2022) Molecular mechanisms of endomembrane trafficking in plants. *Plant Cell*, **34**, 146–173.
- Arpat, A.B., Magliano, P., Wege, S., Rouached, H., Stefanovic, A. & Poirier, Y. (2012) Functional expression of PHO1 to the Golgi and trans-Golgi network and its role in export of inorganic phosphate. *The Plant Journal*, **71**, 479–491.
- Aung, K., Lin, S.-I., Wu, C.-C., Huang, Y.-T., Su, C. & Chiou, T.-J. (2006) *pho2*, a phosphate overaccumulator, is caused by a nonsense mutation in a MicroRNA399 target gene. *Plant Physiology*, **141**, 1000–1011.
- Baisa, G.A., Mayers, J.R. & Bednarek, S.Y. (2013) Budding and braking news about clathrin-mediated endocytosis. *Current Opinion in Plant Biology*, **16**, 718–725.
- Barberon, M., Dubeaux, G., Kolb, C., Isono, E., Zelazny, E. & Vert, G. (2014) Polarization of IRON-REGULATED TRANSPORTER 1 (IRT1) to the plant-soil interface plays crucial role in metal homeostasis. *Proceedings of the National Academy of Sciences of the United States of America*, **111**, 8293–8298.
- Barberon, M. & Geldner, N. (2014) Radial transport of nutrients: the plant root as a polarized epithelium. *Plant Physiology*, **166**, 528–537.
- Barberon, M., Zelazny, E., Robert, S., Conéjéro, G., Curie, C., Friml, J. *et al.* (2011) Monoubiquitin-dependent endocytosis of the IRON-REGULATED TRANSPORTER 1 (IRT1) transporter controls iron uptake in plants. *Proceedings of the National Academy of Sciences of the United States of America*, **108**, E450–E458.
- Bari, R., Datt Pant, B., Stitt, M. & Scheible, W.-R. (2006) PHO₂, MicroRNA399, and PHR1 define a phosphate-signaling pathway in plants. *Plant Physiology*, **141**, 988–999.
- Barthes, L., Bousser, A., Hoarau, J. & Deleens, E. (1995) Reassessment of the relationship between nitrogen supply and xylem exudation in detopped maize seedlings. *Plant Physiology and Biochemistry*, **33**, 173–183.
- Bashline, L., Li, S., Anderson, C.T., Lei, L. & Gu, Y. (2013) The endocytosis of cellulose synthase in *Arabidopsis* is dependent on μ 2, a clathrin-mediated endocytosis adaptin. *Plant Physiology*, **163**, 150–160.
- Bashline, L., Li, S., Zhu, X. & Gu, Y. (2015) The TWD40-2 protein and the AP2 complex cooperate in the clathrin-mediated endocytosis of cellulose synthase to regulate cellulose biosynthesis. *Proceedings of the National Academy of Sciences of the United States of America*, **112**, 12870–12875.
- Bayle, V., Arrighi, J.-F., Creff, A., Nespoulous, C., Vialaret, J., Rossignol, M. *et al.* (2011) *Arabidopsis thaliana* high-affinity phosphate transporters exhibit multiple levels of posttranslational regulation. *Plant Cell*, **23**, 1523–1535.
- Bolte, S. & Cordelières, F.P. (2006) A guided tour into subcellular colocalization analysis in light microscopy. *Journal of Microscopy*, **224**, 213–232.
- Cardona-López, X., Cuyas, L., Marin, E., Rajulu, C., Irigoyen, M.L., Gil, E. *et al.* (2015) ESCRT-III-associated protein ALIX mediates high-affinity phosphate transporter trafficking to maintain phosphate homeostasis in *Arabidopsis*. *Plant Cell*, **27**, 2560–2581.
- Castangs, L., Alcon, C., Kosuth, T., Correia, D. & Curie, C. (2021) Manganese triggers phosphorylation-mediated endocytosis of the *Arabidopsis* metal transporter NRAMP1. *The Plant Journal*, **106**, 1328–1337.
- Chao, Z.-F., Wang, Y.-L., Chen, Y.-Y., Zhang, C.-Y., Wang, P.-Y., Song, T. *et al.* (2021) NPF transporters in synaptic-like vesicles control delivery of iron and copper to seeds. *Science Advances*, **7**, eabh2450.
- Chen, X., Irani, N.G. & Friml, J. (2011) Clathrin-mediated endocytosis: the gateway into plant cells. *Current Opinion in Plant Biology*, **14**, 674–682.
- Clough, S.J. & Bent, A.F. (1998) Floral dip: a simplified method for agrobacterium-mediated transformation of *Arabidopsis thaliana*. *The Plant Journal*, **16**, 735–743.
- Collins, B.M., McCoy, A.J., Kent, H.M., Evans, P.R. & Owen, D.J. (2002) Molecular architecture and functional model of the endocytic AP2 complex. *Cell*, **109**, 523–535.
- Cubero, B., Nakagawa, Y., Jiang, X.Y., Miura, K.J., Li, F., Raghoshama, K.G. *et al.* (2009) The phosphate transporter PHT4;6 is a determinant of salt tolerance that is localized to the Golgi apparatus of *Arabidopsis*. *Molecular Plant*, **2**, 535–552.
- Curtis, M.D. & Grossniklaus, U. (2003) A gateway cloning vector set for high-throughput functional analysis of genes in *planta*. *Plant Physiology*, **133**, 462–469.
- Delhaize, E., Gruber, B.D., Pittman, J.K., White, R.G., Leung, H., Miao, Y. *et al.* (2007) A role for the *AtMTP11* gene of *Arabidopsis* in manganese transport and tolerance. *The Plant Journal*, **51**, 198–210.
- Dhonukshe, P., Aniento, F., Hwang, I., Robinson, D.G., Mravec, J., Stierhof, Y.-D. *et al.* (2007) Clathrin-mediated constitutive endocytosis of PIN auxin efflux carriers in *Arabidopsis*. *Current Biology*, **17**, 520–527.
- Di Rubbo, S., Irani, N.G., Kim, S.Y., Xu, Z.-Y., Gadeyne, A., Dejonghe, W. *et al.* (2013) The clathrin adaptor complex AP-2 mediates endocytosis of BRASSINOSTEROID INSENSITIVE1 in *Arabidopsis*. *Plant Cell*, **25**, 2986–2997.
- Dissanayaka, D.M.S.B., Ghahremani, M., Siebers, M., Wasaki, J. & Plaxton, W.C. (2021) Recent insights into the metabolic adaptations of phosphorus-deprived plants. *Journal of Experimental Botany*, **72**, 199–223.
- Dubeaux, G. & Vert, G. (2017) Zooming into plant ubiquitin-mediated endocytosis. *Current Opinion in Plant Biology*, **40**, 56–62.
- Fan, L., Hao, H., Xue, Y., Zhang, L., Song, K., Ding, Z. *et al.* (2013) Dynamic analysis of *Arabidopsis* AP2 σ subunit reveals a key role in clathrin-mediated endocytosis and plant development. *Development*, **140**, 3826–3837.
- Fuji, K., Miwa, K. & Fujiwara, T. (2009) The intracellular transport of transporters: membrane trafficking of mineral transporters. *Current Opinion in Plant Biology*, **12**, 699–704.
- Gadeyne, A., Sánchez-Rodríguez, C., Vanneste, S., Di Rubbo, S., Zaubner, H., Vanneste, K. *et al.* (2014) The TPLATE adaptor complex drives clathrin-mediated endocytosis in plants. *Cell*, **156**, 691–704.
- Geldner, N., Dénervaud-Tendon, V., Hyman, D.L., Mayer, U., Stierhof, Y.-D. & Chory, J. (2009) Rapid, combinatorial analysis of membrane compartments in intact plants with a multicolor marker set. *The Plant Journal*, **59**, 169–178.
- Giehl, R.F.H., Laginha, A.M., Duan, F., Rentsch, D., Yuan, L. & von Wirén, N. (2017) A critical role of AMT2;1 in root-to-shoot translocation of ammonium in *Arabidopsis*. *Molecular Plant*, **10**, 1449–1460.
- Grones, P., De Meyer, A., Pleskot, R., Mylle, E., Kraus, M., Vandorpe, M. *et al.* (2022) The endocytic TPLATE complex internalizes ubiquitinated plasma membrane cargo. *Nature Plants*, **8**, 1467–1483.
- Guo, B., Jin, Y., Wussler, C., Blancaflor, E.B., Motes, C.M. & Versaw, W.K. (2008) Functional analysis of the *Arabidopsis* PHT₄ family of intracellular phosphate transporters. *The New Phytologist*, **177**, 889–898.
- Gutiérrez-Alanis, D., Ojeda-Rivera, J.O., Yong-Villalobos, L., Cárdenas-Torres, L. & Herrera-Estrella, L. (2018) Adaptation to phosphate scarcity: tips from *Arabidopsis* roots. *Trends in Plant Science*, **23**, 721–730.
- Hamburger, D., Rezzonico, E., MacDonald-Comber Petétot, J., Somerville, C. & Poirier, Y. (2002) Identification and characterization of the *Arabidopsis* PHO1 gene involved in phosphate loading to the xylem. *Plant Cell*, **14**, 889–902.
- Ivanov, R. & Vert, G. (2021) Endocytosis in plants: peculiarities and roles in the regulated trafficking of plant metal transporters. *Biology of the Cell*, **113**, 1–13.
- Jung, J.-Y., Ried, M.K., Hothorn, M. & Poirier, Y. (2018) Control of plant phosphate homeostasis by inositol pyrophosphates and the SPX domain. *Current Opinion in Biotechnology*, **49**, 156–162.
- Karimi, M., Depicker, A. & Hilson, P. (2007) Recombinational cloning with plant gateway vectors. *Plant Physiology*, **145**, 1144–1154.
- Kim, S.Y., Xu, Z.-Y., Song, K., Kim, D.H., Kang, H., Reichardt, I. *et al.* (2013) Adaptor protein complex 2-mediated endocytosis is crucial for male reproductive organ development in *Arabidopsis*. *Plant Cell*, **25**, 2970–2985.
- Kitakura, S., Vanneste, S., Robert, S., Löffke, C., Teichmann, T., Tanaka, H. *et al.* (2011) Clathrin mediates endocytosis and polar distribution of PIN auxin transporters in *Arabidopsis*. *Plant Cell*, **23**, 1920–1931.

- Korbei, B., Moulinier-Anzola, J., De-Araujo, L., Lucyshyn, D., Retzer, K., Khan, M.A. *et al.* (2013) Arabidopsis TOL proteins act as gatekeepers for vacuolar sorting of PIN2 plasma membrane protein. *Current Biology*, **23**, 2500–2505.
- Lee, M.M. & Schiefelbein, J. (1999) WEREWOLF, a MYB-related protein in *Arabidopsis*, is a position-dependent regulator of epidermal cell patterning. *Cell*, **99**, 473–483.
- Li, B., Byrt, C., Qiu, J., Baumann, U., Hrmova, M., Evrard, A. *et al.* (2016) Identification of a stelar-localized transport protein that facilitates root-to-shoot transfer of chloride in *Arabidopsis*. *Plant Physiology*, **170**, 1014–1029.
- Li, R.L., Wang, J.L., Xu, L., Sun, M.H., Yi, K.K. & Zhao, H.Y. (2020) Functional analysis of phosphate transporter OsPHT4 family members in rice. *Rice Science*, **27**, 493–503.
- Li, X., Wang, X., Yang, Y., Li, R., He, Q., Fang, X. *et al.* (2011) Single-molecule analysis of PIP₂:1 dynamics and partitioning reveals multiple modes of *Arabidopsis* plasma membrane aquaporin regulation. *Plant Cell*, **23**, 3780–3797.
- Lin, S.-H., Kuo, H.-F., Canivenc, G., Lin, C.-S., Lepetit, M., Hsu, P.-K. *et al.* (2008) Mutation of the *Arabidopsis* NRT1.5 nitrate transporter causes defective root-to-shoot nitrate transport. *Plant Cell*, **20**, 2514–2528.
- Lin, W.-Y., Huang, T.-K. & Chiou, T.-J. (2013) NITROGEN LIMITATION ADAPTATION, a target of MicroRNA827, mediates degradation of plasma membrane-localized phosphate transporters to maintain phosphate homeostasis in *Arabidopsis*. *Plant Cell*, **25**, 4061–4074.
- Liu, S.-H., Wong, M.L., Craik, C.S. & Brodsky, F.M. (1995) Regulation of clathrin assembly and trimerization defined using recombinant triskelion hubs. *Cell*, **83**, 257–267.
- Liu, T.-Y., Huang, T.-K., Tseng, C.-Y., Lai, Y.-S., Lin, S.-I., Lin, W.-Y. *et al.* (2012) PHO2-dependent degradation of PHO1 modulates phosphate homeostasis in *Arabidopsis*. *Plant Cell*, **24**, 2168–2183.
- Livak, K.J. & Schmittgen, T.D. (2001) Analysis of relative gene expression data using real-time quantitative PCR and the 2^{-ΔΔCT} method. *Methods*, **25**, 402–408.
- Ma, B., Zhang, L., Gao, Q., Wang, J., Li, X., Wang, H. *et al.* (2021) A plasma membrane transporter coordinates phosphate reallocation and grain filling in cereals. *Nature Genetics*, **53**, 906–915.
- McMahon, H.T. & Boucrot, E. (2011) Molecular mechanism and physiological functions of clathrin-mediated endocytosis. *Nature Reviews. Molecular Cell Biology*, **12**, 517–533.
- Moulinier-Anzola, J., Schwihla, M., De-Araujo, L., Artner, C., Jörg, L., Konstantinova, N. *et al.* (2020) TOLs function as ubiquitin receptors in the early steps of the ESCRT pathway in higher plants. *Molecular Plant*, **13**, 717–731.
- Nelson, B.K., Cai, X. & Nebenführ, A. (2007) A multicolored set of *in vivo* organelle markers for co-localization studies in *Arabidopsis* and other plants. *The Plant Journal*, **51**, 1126–1136.
- Nguyen, N.N.T., Clua, J., Vetal, P.V., Vuarambon, D.J., De Bellis, D., Pervent, M. *et al.* (2020) PHO1 family members transport phosphate from infected nodule cells to bacteroids in *Medicago truncatula*. *Plant Physiology*, **185**, 196–209.
- Nussaume, L., Kanno, S., Javot, H., Marin, E., Pochon, N., Ayadi, A. *et al.* (2011) Phosphate import in plants: focus on the PHT1 transporters. *Frontiers in Plant Science*, **2**, 83.
- Paez Valencia, J., Goodman, K. & Otegui, M.S. (2016) Endocytosis and endosomal trafficking in plants. *Annual Review of Plant Biology*, **67**, 309–335.
- Peiter, E., Montanini, B., Gobert, A., Pedas, P., Husted, S., Maathuis, F.J.M. *et al.* (2007) A secretory pathway-localized cation diffusion facilitator confers plant manganese tolerance. *Proceedings of the National Academy of Sciences of the United States of America*, **104**, 8532–8537.
- Poirier, Y., Jaskolowski, A. & Clúa, J. (2022) Phosphate acquisition and metabolism in plants. *Current Biology*, **32**, R623–R629.
- Poirier, Y., Thoma, S., Somerville, C. & Schiefelbein, J. (1991) A mutant of *Arabidopsis* deficient in xylem loading of phosphate. *Plant Physiology*, **97**, 1087–1093.
- Robert, S., Kleine-Vehn, J., Barbez, E., Sauer, M., Paciorek, T., Baster, P. *et al.* (2010) ABP1 mediates auxin inhibition of clathrin-dependent endocytosis in *Arabidopsis*. *Cell*, **143**, 111–121.
- Rodriguez-Furlan, C., Minina, E.A. & Hicks, G.R. (2019) Remove, recycle, degrade: regulating plasma membrane protein accumulation. *Plant Cell*, **31**, 2833–2854.
- Shin, L.-J., Lo, J.-C., Chen, G.-H., Callis, J., Fu, H. & Yeh, K.-C. (2013) IRT1 DEGRADATION FACTOR1, a RING E3 ubiquitin ligase, regulates the degradation of IRON-REGULATED TRANSPORTER1 in *Arabidopsis*. *Plant Cell*, **25**, 3039–3051.
- Siligato, R., Wang, X., Yadav, S.R., Lehesranta, S., Ma, G., Ursache, R. *et al.* (2016) MultiSite gateway-compatible cell type-specific gene-inducible system for plants. *Plant Physiology*, **170**, 627–641.
- Stefanovic, A., Arpat, A.B., Bligny, R., Gout, E., Vidoudez, C., Bensimon, M. *et al.* (2011) Over-expression of PHO1 in *Arabidopsis* leaves reveals its role in mediating phosphate efflux. *The Plant Journal*, **66**, 689–699.
- Stefanovic, A., Ribot, C., Rouached, H., Wang, Y., Chong, J., Belbahri, L. *et al.* (2007) Members of the PHO1 gene family show limited functional redundancy in phosphate transfer to the shoot, and are regulated by phosphate deficiency via distinct pathways. *The Plant Journal*, **50**, 982–994.
- Takano, J., Miwa, K., Yuan, L., von Wiren, L. & Fujiwara, T. (2005) Endocytosis and degradation of BOR1, a boron transporter of *Arabidopsis thaliana*, regulated by boron availability. *Proceedings of the National Academy of Sciences of the United States of America*, **102**, 12276–12281.
- Takano, J., Noguchi, K., Yasumori, M., Kobayashi, M., Gajdos, Z., Miwa, K. *et al.* (2002) *Arabidopsis* boron transporter for xylem loading. *Nature*, **420**, 337–340.
- Van Damme, D., Coutuer, S., De Rycke, R., Bouget, F.-Y., Inzé, D. & Geelen, D. (2007) Somatic cytokinesis and pollen maturation in *Arabidopsis* depend on TPLATE, which has domains similar to coat proteins. *Plant Cell*, **18**, 3502–3518.
- Vogiatzaki, E., Baroux, C., Jung, J.-Y. & Poirier, Y. (2017) PHO1 exports phosphate from the chalazal seed coat to the embryo in developing *Arabidopsis* seeds. *Current Biology*, **27**, 2893–2900.
- Wang, Q., Zhao, Y., Luo, W., Li, R., He, Q., Fang, X. *et al.* (2013) Single-particle analysis reveals shutoff control of the *Arabidopsis* ammonium transporter AMT1;3 by clustering and internalization. *Proceedings of the National Academy of Sciences of the United States of America*, **110**, 13204–13209.
- Wege, S., Khan, G.A., Jung, J.-Y., Vogiatzaki, E., Pradervand, S., Aller, I. *et al.* (2016) The EXS domain of PHO1 participates in the response of shoots to phosphate deficiency via a root-to-shoot signal. *Plant Physiology*, **170**, 385–400.
- Wild, R., Gerasimaite, R., Jung, J.-Y., Truffault, V., Pavlovic, I., Schmidt, A. *et al.* (2016) Control of eukaryotic phosphate homeostasis by inositol polyphosphate sensor domains. *Science*, **352**, 986–990.
- Yamaoka, S., Shimono, Y., Shirakawa, M., Fukao, Y., Kawase, T., Hatsugai, N. *et al.* (2013) Identification and dynamics of *Arabidopsis* adaptor protein-2 complex and its involvement in floral organ development. *Plant Cell*, **25**, 2958–2969.
- Yoshinari, A., Hosokawa, T., Amano, T., Beier, M.P., Kunieda, T., Shimada, T. *et al.* (2019) Polar localization of the borate exporter BOR1 requires AP2-dependent endocytosis. *Plant Physiology*, **179**, 1569–1580.
- Zelazny, E. & Vert, G. (2014) Plant nutrition: root transporters on the move. *Plant Physiology*, **166**, 500–508.
- Zhang, Z., Liao, H. & Lucas, W.J. (2014) Molecular mechanisms underlying phosphate sensing, signaling, and adaptation in plants. *Journal of Integrative Plant Biology*, **56**, 192–220.
- Zhou, F., Emonet, A., Dénervaud Tendon, V., Marhavy, P., Wu, D., Lahaye, T. *et al.* (2020) Co-occurrence of damage and microbial patterns controls localized immune responses in roots. *Cell*, **180**, 440–453.